applied sciences

MDPI

Review

Optical Accelerometers for Detecting Low-Frequency Micro-Vibrations

Ying-Jun Lei [1,2], Rui-Jun Li [1,2,*], Lian-Sheng Zhang [1,2,*], Peng-Hao Hu [1,2] and Qiang-Xian Huang [1,2]

[1] School of Instrument Science and Opto-Electronics Engineering, Hefei University of Technology, Hefei 230009, China; 2016170008@mail.hfut.edu.cn (Y.-J.L.); hupenghao@hfut.edu.cn (P.-H.H.); huangqx@hfut.edu.cn (Q.-X.H.)

[2] Anhui Province Key Laboratory of Measuring Theory and Precision Instrument, Hefei University of Technology, Hefei 230009, China

* Correspondence: rj-li@hfut.edu.cn (R.-J.L.); lszhang@hfut.edu.cn (L.-S.Z.)

Abstract: Optical accelerometers are high-precision inertial sensors that use optical measurement technology to achieve high-precision and electromagnetic interference-resistant acceleration measurements. With the intensive research and development of optical accelerometers in recent years, their applications in inertial navigation, structural health monitoring, precision vibration isolation systems, wind turbine fault monitoring, earthquake monitoring, and other low-frequency vibration detection have flourished. Optical accelerometers have various schemes; however, their characteristics vary considerably due to different optical modulation schemes. This study aims to address the lack of systematic evaluation of currently available low-frequency optical accelerometers. Optical accelerometers can be classified into four categories in accordance with their optical modulation schemes: optical path-, optical intensity-, optical phase-, and optical wave-length-modulated accelerometers. The typical performance, advantages and disadvantages, and possible application scenarios of various optical accelerometers are summarized. This study also presents the current status and trends of low-frequency optical accelerometers in consideration of the growing demand for high-precision, low-frequency acceleration measurements.

Keywords: accelerometer; optical sensing systems; optical modulation; accelerometer review

check for updates

Citation: Lei, Y.-J.; Li, R.-J.; Zhang, L.-S.; Hu, P.-H.; Huang, Q.-X. Optical Accelerometers for Detecting Low-Frequency Micro-Vibrations. *Appl. Sci.* **2022**, *12*, 3994. https://doi.org/10.3390/app12083994

Academic Editors: Guanhao Wu, Xiuguo Chen and Yuki Shimizu

Received: 22 March 2022
Accepted: 13 April 2022
Published: 14 April 2022

1. Introduction

Vibration is closely related to people's daily life and production, and thus, vibration detection is highly significant. The parameters of vibration signals include displacement, velocity, and acceleration. Vibration detection can be achieved by measuring the values of these parameter quantities. Accelerometers are efficient instruments for vibration detection.

Accelerometers can be categorized into electronic and optical accelerometers in accordance with their operating principles. Electronic accelerometers include piezoelectric, capacitive, and piezoresistive types. Piezoelectric accelerometers have many advantages, such as low cost, availability in many forms, and simplicity in handling and implementation; however, they exhibit the problems of low linearity and accuracy caused by external excitation and the piezoelectric material [1,2]. Capacitive accelerometers present the advantages of high sensitivity, low frequency response, and wide dynamic range. However, they can be easily interfered with by the external environment and are only suitable for low-frequency field applications, such as seismic detection and geological exploration [3,4]. Piezoresistive acceleration sensors demonstrate the advantages of small volume, low output impedance, and high measurement accuracy; however, they are easily affected by temperature [5,6]. In addition to the above factors, piezoelectric, piezoresistive, and capacitive accelerometers are vulnerable to electromagnetic interference due to the limitations of their sensing principles, making it difficult to detect micro-vibrations.

Compared with electrical sensing, optical sensing improves the sensitivity of accelerometers by an order of magnitude and enables accurate detection of micro-vibrations [7]. Various optical accelerometers have been reported in the past decades, yet a systematic review of low-frequency optical accelerometers has remained elusive. In this review, we focus on the measurement principle and performance of state-of-the-art optical accelerometers and divide them into several categories in accordance with their optical modulation scheme. By using typical demonstrations as examples, merits and disadvantages are presented here, providing a big picture of optical accelerometers, along with their application prospects and development tendencies.

2. Principle and Requirements

2.1. Principle of Accelerometer

A common accelerometer comprises a spring, a damper, a seismic mass, and a displacement sensor arranged within a housing attached to a base [8], as shown in Figure 1. In operation, the base is mounted on the vibrating structure to be measured, and the relative displacement between the seismic mass and the base is recorded by the displacement sensor.

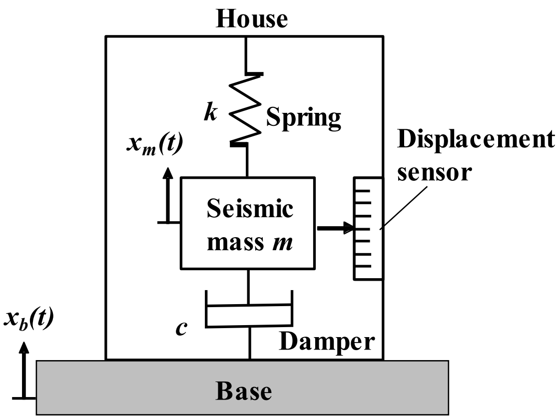

Figure 1. Typical accelerometer structure diagram.

Following Newton's second law, the force acting on the seismic mass m can be expressed as

$$ma = -k(x_m - x_b) - c(\dot{x}_m - \dot{x}_b), \tag{1}$$

where x_m is the displacement of the seismic mass, x_b is the displacement of the base, a is the acceleration to be detected, k is the elastic coefficient of spring, and c is the damper coefficient of the accelerometer. The relative displacement z between the seismic mass and the base can be expressed as

$$z(t) = x_m(t) - x_b(t). \tag{2}$$

Assuming the detected vibration is a simple harmonic vibration, we have $x_b(t) = X_b \cos(\omega_b t)$, where ω_b is the frequency of vibration. Bring $x_b(t)$ and $z(t)$ into Equation (1):

$$m\ddot{z} + c\dot{z} + kz = m\omega_b^2 X_b \cos \omega_b t. \tag{3}$$

Solve Equation (3) and obtain:

$$z(t) = \left[1 \middle/ \left(\sqrt{(\omega_n^2 - \omega_b^2)^2 + (2\xi\omega_n\omega_b)^2}\right)\right] * \left[\omega_b^2 X_b \cos(\omega_b t - \varphi)\right], \tag{4}$$

where $\omega_n = (k/m)^{1/2}$ is the resonant frequency of the accelerometer, $\xi = c/2(m\omega_n)$ is the damping ratio of the accelerometer, and φ can be expressed as

$$\varphi = \tan^{-1}\left[(2\xi(\omega_b/\omega_n)) \middle/ \left(1 - (\omega_b/\omega_n)^2\right)\right]. \tag{5}$$

Additionally, the acceleration caused by vibration is

$$\ddot{x}_b(t) = -\omega_b^2 X_b \cos(\omega_b t). \tag{6}$$

Equation (4) can be rewritten as

$$\omega_n^2 z(t) = \left[1 \Big/ \left(\sqrt{(1-(\omega_b^2/\omega_n^2)^2 + (2\xi\omega_b/\omega_n)^2}\right)\right] * \left[\omega_b^2 X_b \cos(\omega_b t - \varphi)\right] \tag{7}$$

Order

$$H(\omega_b/\omega_n) = 1 \Big/ \left(\sqrt{(1-(\omega_b^2/\omega_n^2)^2 + (2\xi\omega_b/\omega_n)^2}\right). \tag{8}$$

When $\omega_b \ll \omega_n$, the $H(\omega_b/\omega_n) \approx 1$ and $\varphi \approx 0$. Then the acceleration value $\ddot{x}_b$ can be calculated as

$$\ddot{x}_b \approx \omega_n^2 z(t). \tag{9}$$

As can be seen from Equation (9), the mechanical sensitivity of the accelerometer can be approximated as the inverse of the square of its resonant frequency, so the higher the resonant frequency, the lower the mechanical sensitivity. Therefore, the low frequency accelerometer needs to have a lower resonant frequency. Additionally, the use of high-sensitivity displacement sensors can also improve the sensitivity of accelerometers.

2.2. Requirements of Low Frequency Accelerometers

Low-frequency, high-sensitivity accelerometers have a wide range of applications, and they play an important role in industries and daily life, including inertial navigation, structural health monitoring, active vibration isolation systems, fault detection of wind turbine, and earthquake detection.

2.2.1. Inertial Navigation

Navigation techniques are divided into two categories: positioning and trajectory extrapolation [9]. One representative of positioning technology is a global navigation satellite system. The trajectory extrapolation method recursively measures the amount of variation in the real-time motion state of a moving object relative to the initial motion state. Then, the real-time position of the moving object based on that amount of change is determined. Inertial navigation is an example of the trajectory extrapolation method used as a navigation technique. An accelerometer in an inertial navigation system can measure the acceleration and angular acceleration of the carrier. In accordance with Newton's second law of motion, time integrates acceleration and angular acceleration to obtain the velocity, angular velocity, and position information of a moving object. The operation of time integration will amplify the error of the accelerometer, and thus, an accelerometer used in an inertial navigation system must meet high accuracy, stability, and anti-interference capability requirements. Optical accelerometers exhibit advantages in terms of accuracy, stability, and immunity to electromagnetic interference by utilizing optical sensing. They demonstrate good prospects in inertial navigation.

2.2.2. Structural Health Monitoring

Bridges vibrate when vehicles pass over them, and high buildings sway when strong winds blow around them. If the vibration of large buildings exceeds the threshold value, catastrophic losses may occur. Accelerometers can measure the structural vibration of these buildings to determine their structural health and provide early warning for potential damage. Structural vibrations in large buildings are typically low-frequency vibrations below 100 Hz, and they require a multipoint arrangement for monitoring. Therefore, accelerometers must achieve high accuracy with a small size and meet the requirements for long-distance measurement [10]. An optical sensor-based accelerometer has high measurement accuracy while enabling long-distance and distributed measurements; thus, it can meet the structural health monitoring needs of large buildings [11].

2.2.3. Vibration Isolation Systems

In microscale and nanoscale precision measurement systems and ultra-precision machining systems, the effects of vibration on measurement precision and machining accuracy is devastating, and the vibration is a major factor that limits the improvement of measurement and machining accuracy [12,13]. Vibration isolation is divided into active and passive vibration isolations; passive vibration isolation techniques experience difficulty in isolating low-frequency vibrations of 0.5–5 Hz [14], while active vibration isolation can suppress low-frequency vibrations more efficiently. In an active vibration control system, accurate access to real-time vibration information is the key. Therefore, high-precision real-time detection of low-frequency micro-vibrations must be inevitably achieved. Optical accelerometers demonstrate advantages in measurement accuracy and response speed. They have potential applications in the field of precision active vibration isolation.

2.2.4. Fault Detection of Wind Turbine

Wind energy has grown rapidly in the last decade due to its clean and renewable nature. By the end of 2021, more than 650 GW of installed wind energy capacity has been put into operation worldwide. Mechanical drive components (gears and bearings) of wind turbines are prone to failure due to exposure to harsh environments, such as random winds, temperature differences, and alternating loads [15–17]. Mechanical failures of wind turbines may lead to their shutdown and have adverse social impacts. Therefore, the study of mechanical failure detection of wind turbine units has received increasing attention develop a reasonable operation and maintenance plan and to avoid catastrophic consequences. The lowest rotational frequency of the internal rotating mechanism of a wind turbine can be as low as 0.33 Hz [18], so the fault detection accelerometer of a wind turbine needs to have good low-frequency response characteristics, as well as high sensitivity.

2.2.5. Earthquake Monitoring

Advances in seismology have relied closely on the development of instruments. From a scientific point of view, accuracy is crucial: the more accurate the detection of seismic properties, the more reliable the understanding of earthquake hazards, which in turn is of guiding importance for the study of seismic prevention techniques. In addition to seismic research, monitoring of earthquakes is also used in resource exploration, gravity-assisted navigation, and monitoring of volcanic activity. According to previous studies, the frequency range of the Earth's near-source strong ground motions is 0.3–3.0 Hz [19]; therefore, earthquake monitoring accelerometers need to have good low-frequency response characteristics.

3. Optical Path Modulation

An optical accelerometer based on the optical path modulation principle senses acceleration by directly modulating the optical path. When external acceleration acts on the accelerometer, seismic mass in the accelerometer is inertially displaced, directly altering the laser optical path. This type of accelerometer exhibits the advantages of a simple structure and low cost.

A focus error sensor (FES) based on a DVD pickup head is a high-precision optical path modulation sensing system. Figure 2 shows a focus sensor modified from a red-ray DVD pickup head by removing the voice coil motor and using a rectangular prism to turn the optical path. It exhibits the advantages of high resolution and high accuracy. This modified sensor can be used in nanoscale measurement after calibration. As shown in Figure 3a, Chu et al. designed a cantilevered high-sensitivity optical accelerometer with a sensitivity of 12.3 V/g on the basis of focus error sensing [20]. As shown in Figure 3b, Liu et al. improved the design of Chu et al. by using the moving part of the voice coil motor inside a DVD pickup head as the elastic mechanism; they reduced the size of the accelerometer while improving its sensitivity to 24.4 V/g [21]. The resonant frequency in the x and y directions of a cantilevered beam is not significantly greater than the resonant frequency in the z-direction, and vibrations in the x and y directions exert a greater effect on the output of the accelerometer. Therefore, Li et al. designed an accelerometer with a fully symmetric leaf spring (as shown in Figure 4); it has a resolution of 0.3 mg and measurement uncertainty as low as 0.07 mg (K = 2) [22]. To improve the sensitivity of optical accelerometers, Cheng et al. modeled an optical accelerometer by using sensitivity analysis and improved its sensing optical path to achieve a resolution as low as 4 μg [23].

The FES is based on a modified DVD pickup head, and its internal optical components are irreplaceable and exhibit poor maintainability. Laser triangulation (LTG) is a method for achieving position detection on the basis of the change in optical path. As depicted in Figure 5, when the position of the reflector changes Δh, the position of the spot on the photodetector will also change Δl. The relationship between Δh and Δl is

$$\Delta l = \frac{\Delta h}{\sin \alpha}, \tag{10}$$

where α is the angle between the incident laser beam and the reflector. Therefore, the LTG method can amplify the displacement $1/\sin \alpha$ times. This method is widely used in micro/nano measurement instruments, such as micro/nano contact probes [24], scanning probe microscopes [25], and optical accelerometers (Figure 6) [7]. With the development of technology, the resolution of photodetectors has reached the submicron order. For example, the photodetector (SPOT-4, OSI Optoelectronics Co., Ltd., Hawthorne, CA, USA) used in the literature [7] has a position resolution of 0.1 μm, and with optical lever amplification; this displacement sensor has a resolution of 70 nm. An optical accelerometer based on the LTG method and a fully symmetrical leaf spring-type elastic mechanism can achieve a low-frequency response down to 0.4 Hz and a high resolution of 0.3 mg.

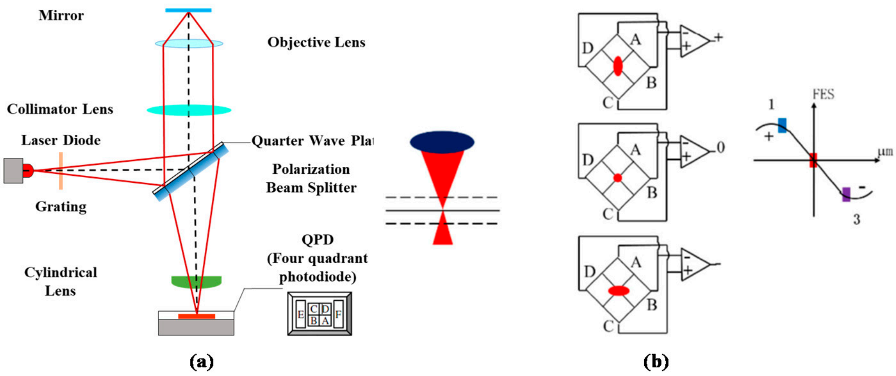

Figure 2. FES: (**a**) structure schematic and (**b**) sensing principle. Reprinted with permission from Ref. [26]. Copyright 2019 Springer Nature.

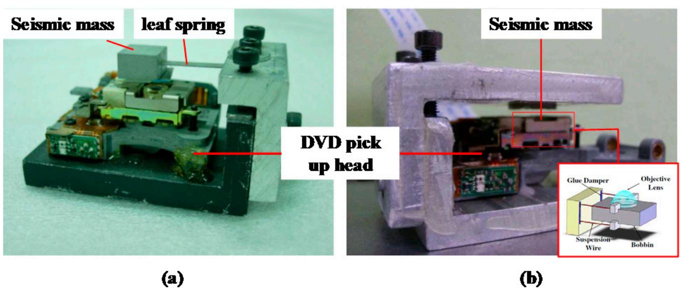

Figure 3. Cantilevered accelerometers: (**a**) leaf spring and (**b**) voice coil. Reprinted with permission from Ref. [21]. Copyright 2008 IOP.

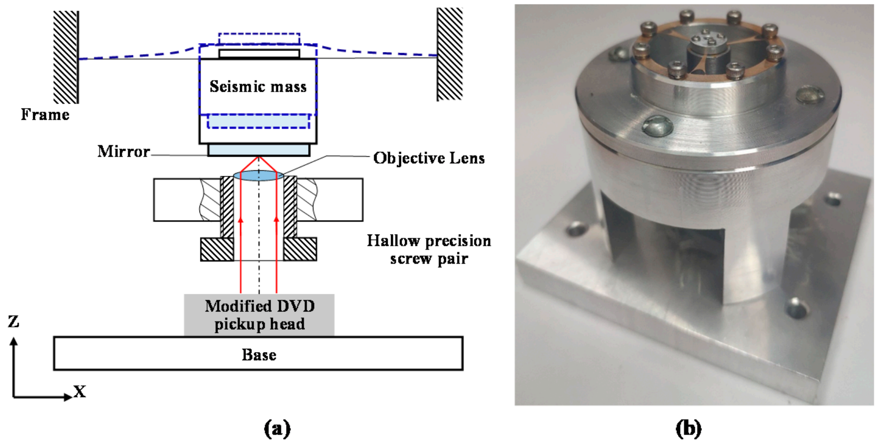

Figure 4. Accelerometer with a fully symmetric leaf spring: (**a**) structure schematic and (**b**) photograph. Reprinted with permission from Ref. [22]. Copyright 2019 IEEE.

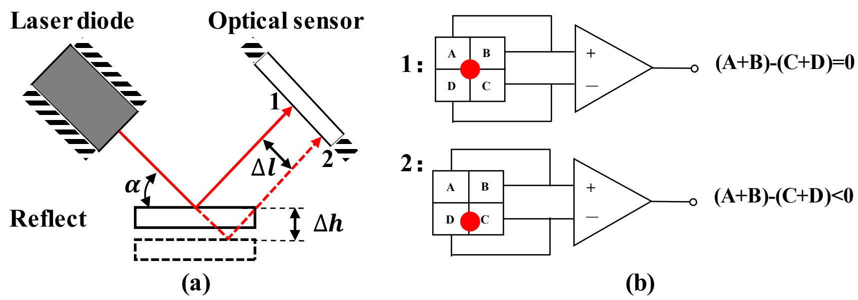

Figure 5. Principle of LTG: (**a**) optical path and (**b**) output signal.

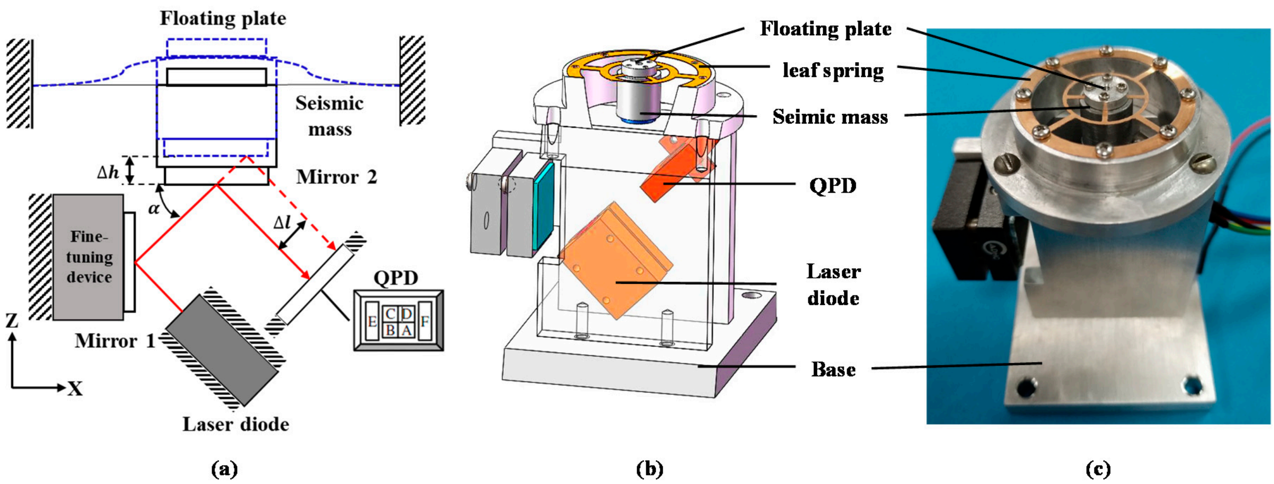

Figure 6. Accelerometer based on the LTG [7]: (**a**) principle, (**b**) structure schematic, and (**c**) photograph.

Common 1D accelerometers cannot meet the requirements of the aerospace, robotics, and other multidimensional measurement fields due to the complexity and multidimensionality of vibration. Therefore, research on 2D accelerometers has been increasing gradually. The key to 2D optical accelerometers is 2D angle sensing. Figure 7a presents the schematic of a 2D angle sensor modified from a DVD pickup head [26]. As shown in Figure 7b, Chu et al. designed a highly sensitive 2D optical accelerometer based on a modified DVD pickup head with x- and y-axis sensitivities of 22.9 V/g and 21.3 V/g, respectively [27].

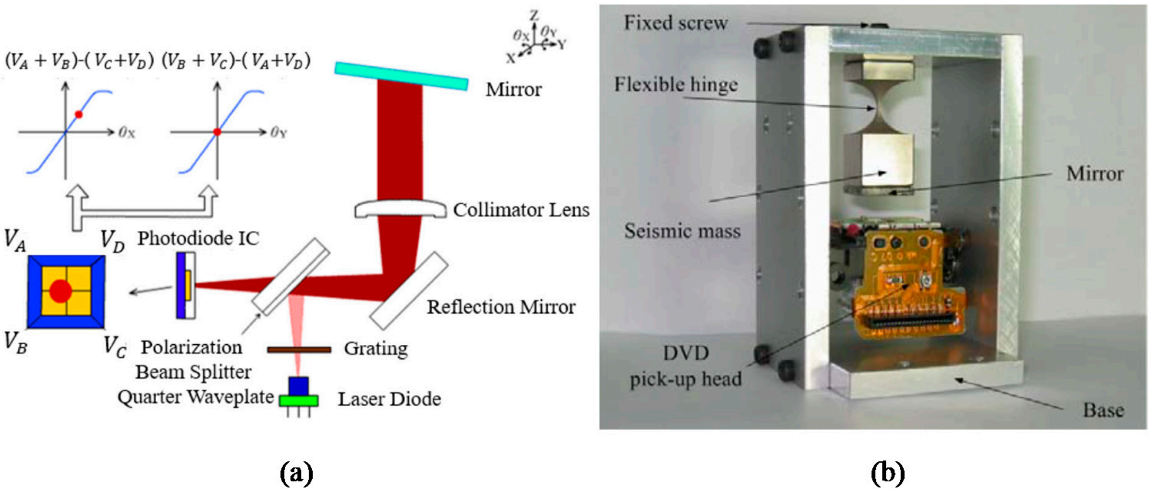

Figure 7. Accelerometer based on the LAC: (**a**) 2D angle sensor and (**b**) 2D accelerometer based on a DVD pickup head. Figure (**a**) is reprinted with permission from Ref. [26]. Copyright 2019 Springer Nature.

Although the use of a DVD pickup head is convenient; this part is extremely compact, such that any component change is impossible. Following the optical configuration of a DVD pickup head, a compact 2D angle sensor based on the laser autocollimator (LAC) principle was developed to expand the measurement range [28]. Lei et al. designed a 2D optical accelerometer based on this modified 2D angle sensor [29] (Figure 8). The accelerometer uses a hollow cylindrical arc-cut 2D flexure hinge, which references its stability, and is based on an optical sensing method, which imbues it with high sensitivity and resolution. Its *x*- and *y*-axis sensitivities are 25.2 V/g and 25.6 V/g, respectively, and its test resolution is down to 60 µg. Compared with that in Chu et al., the performance and serviceability of this optical accelerometer are improved, enhancing its application value.

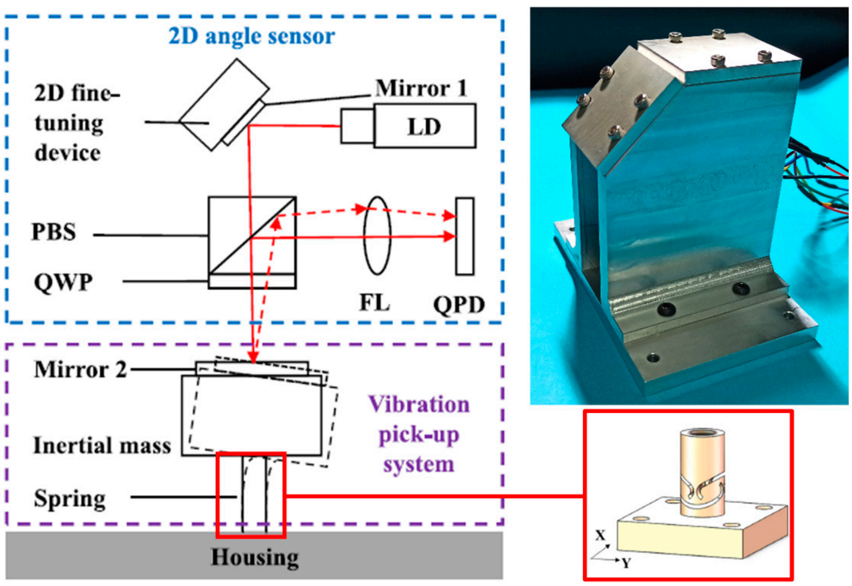

Figure 8. 2D accelerometer based on a modified 2D angle sensor. Reprinted with permission from Ref. [26]. Copyright 2021 Elsevier.

In addition to 2D angle sensors based on the LAC principle, 2D angle measurement based on the laser interference (LI) principle was proposed by Fang et al. This method utilizes the spectral separation properties of angular cone prisms and gratings with directional reflection characteristics to achieve a coherent beam with an error of less than ±0.01°

for 2D angle measurement. On the basis of this principle, Fang et al. designed a 2D optical accelerometer that can reach a measurement range of 177 g with a measurement error of less than 0.1 g [30]. This study achieved a large range but sacrificed measurement accuracy.

In summary, optical accelerometers based on optical path modulation are characterized by a simple structure and convenient signal processing; high sensitivity can be achieved by optimizing the mechanical [22] or optical sensing units [23]. However, the measurement accuracy of this type of optical accelerometer is directly related to the structure of the optical path and the performance of the photodetector. To increase the sensitivity of the accelerometer, the optical range of the optical lever should be widened, and a high-sensitivity photodetector should be used, increasing the size and cost of the accelerometer. The parameters of the structures and the optical accelerometer based on optical path modulation (i.e., resonant frequency, working frequency band, and sensitivity) are provided in Table 1.

Table 1. Parameters of the accelerometer based on optical path modulation.

Reference	Principle	Structure	Resonant Frequency (Hz)	Frequency Response Range (Hz)	Sensitivity
Chu et al. [20]	FES	Cantilevered leaf spring	130	0.5–24	12.3 V/g
Liu et al. [21]	FES	Cantilevered wire spring	53	3–8	24.4 V/g
Li et al. [22]	FES	Fully symmetrical leaf spring	46.5	1–10	10.8 V/g
Cheng et al. [23]	FES	Fully symmetrical leaf spring	49.3	0.7–11	192.1 V/g
Li et al. [7]	LTG	Fully symmetrical leaf spring	45	0.4–12	17.4 V/g
Chu et al. [27]	LAC	Flexure hinge	X: 92.8 Y: 92.9	0.5–24	X: 22.9 V/g, Y: 21.3 V/g
Lei et al. [29]	LAC	Arc-cut flexure hinge	X: 44.2 Y: 40.0	0.8–10	X: 25.2 V/g, Y: 25.6 V/g
Fang et al. [30]	LI	Hanging thread	–	–	13.5 s^2

4. Optical Intensity Modulation

An optical accelerometer based on optical intensity modulation is a type of accelerometer that senses acceleration by directly modulating the radiation intensity of light. Given that it is subject to acceleration, seismic mass in the accelerometer generates an inertial displacement that directly changes output optical intensity. In conjunction with the acceleration–displacement sensitivity of the acceleration sensing structure, the magnitude of the input acceleration can be calculated from the change in the output light intensity of the accelerometer. This type of optical accelerometers exhibits the advantages of a simple structure and low cost. However, guaranteeing its precision is typically difficult due to its relatively high susceptibility to the fluctuation of the incident light source and the external environment.

The simplest optical accelerometer with optical intensity modulation is the optical waveguide (OWG) accelerometer. As shown in Figure 9a, Kalenik et al. and Barbosa et al. fixed a transmitting fiber in the form of a cantilever beam at one end and a receiving fiber at the other end [31,32]. When acceleration acts on this structure, the cantilever beam bends, reducing the optical flux of the receiving fiber. The acceleration value can be obtained from the change in this flux. Lee et al. improved the design by not using the optical fiber directly as the pickup component, and instead, using a symmetrical elastic structure (Figure 9b), in which the mass block drives the shutter to move, and the movement of the shutter causes the light flux to change [33]. Llobera et al. further enhanced the design of Lee et al. A fish bone-shaped self-aligning pickup mechanism based on microelectromechanical system (MEMS) processing technology was designed to simplify the initial fiber alignment problem [34,35]. The OWG-based accelerometer exhibits the advantages of a simple structure and low cost; however, its application is limited by its high environmental sensitivity and low accuracy [36,37].

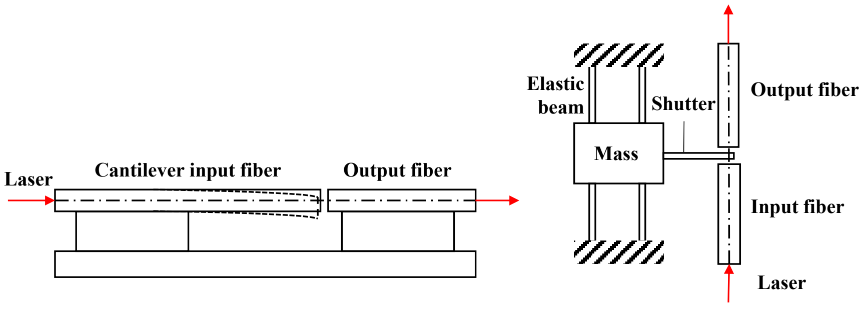

(a) (b)

Figure 9. OWG accelerometer: (**a**) cantilever type and (**b**) shutter type.

In addition to OWG, grating shutters (GSs) can also be used as optical intensity modulation elements for accelerometers. Abbaspour et al. proposed a GS-based accelerometer, the light source emits light vertically downward, with a GS-shaped sensing structure in the middle and a grating-type detector below, along with a detector for sensing ambient light, achieving common-mode rejection. The linear range of this accelerometer reaches ±84 g, but its sensitivity is less than 0.1 V/g [38]. Wu et al. fabricated an optical accelerometer with a wide band of 10 Hz–1.5 kHz on the basis of MEMS technology with an array of gratings with square holes, an array of organic light-emitting diodes as the light source, and an array of organic photodetectors as the detector [39]. Similarly, Carr et al. fabricated a high-precision sub-wavelength nano-grating based on photolithography and designed a wide-band high-sensitivity displacement sensor based on this grating and an arrayed vertical cavity surface laser [40,41]. Krishnamoorthy et al. applied the grating to a high-sensitivity optical accelerometer, as shown in Figure 10. This optical accelerometer achieves a resonant frequency of 36 Hz and a sensitivity of 590 V/g [42].

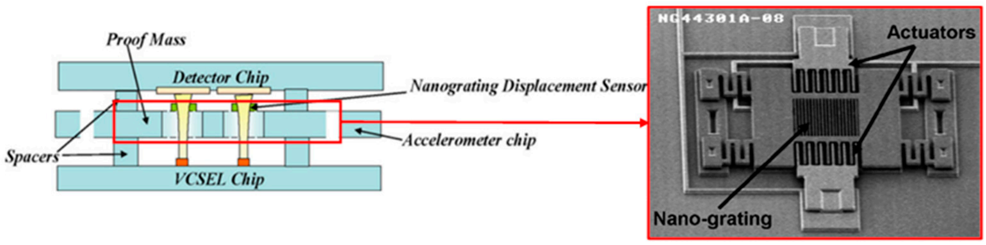

Figure 10. GS-based accelerometer. Reprinted with permission from Ref. [42]. Copyright 2008 Elsevier.

Similar to the principle of GS, an optical shadow sensor (OSS) realizes sensing by detecting changes in shadows projected onto the photosensitive surface of a photodetector [43]. Bochobza et al. used an OSS to measure the motion of seismic mass, as shown in Figure 11a [44,45]. The system consists of a suspended seismic mass and a complementary metal–oxide–semiconductor (CMOS) chip with a detection photodiode and a readout circuit. When acceleration acts on the system, the seismic mass moves, causing a change in the shaded portion of the CMOS chip's photosensitive surface, which, in turn, causes a change in the chip's output signal, from which the acceleration value can be calculated. The performance of the accelerometer is affected by the resolving power of the CMOS chip at the micron level. Hammond et al. used high-sensitivity photodetectors instead of CMOS chips to improve the accuracy of OSS [46]. This photodetector is produced by Siemens, model BPX-65, and has a sensitivity of 0.55 A/W, a quantum efficiency of 80%, and a NEP of 3.3×10^{-14} W/Hz$^{1/2}$. The accelerometer designed by Hammond et al. also uses an inverse spring with a very low resonance frequency (2.3 Hz) with an accelerometer sensitivity as low as 41 ng/Hz$^{1/2}$. Tang et al. and Duan et al. also designed accelerometers with very low resonant frequencies [47,48]. Tang et al. used an asymmetric spring structure that consisted of two curved and two folded beams, as shown in Figure 11b, to significantly improve the sensitivity of the optical accelerometer to 8.1 ng/Hz$^{1/2}$.

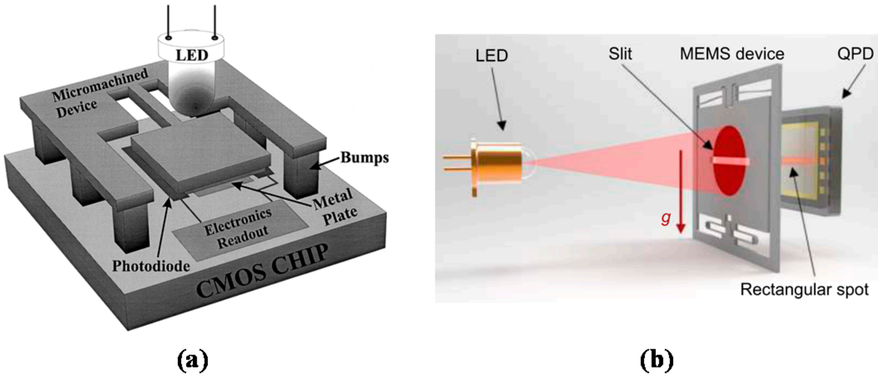

Figure 11. OSS-based accelerometer: (**a**) cantilevered and (**b**) asymmetric spring. Figures are reprinted with permission from: (**a**) Ref. [44]. Copyright 2000 Elsevier; (**b**) Ref. [47]. Copyright 2019 Springer Nature.

In summary, optical accelerometers based on optical intensity modulation are similar to those based on optical path modulation, with a simple structure and lower cost. This type of optical accelerometers can achieve extremely high sensitivity by using a highly sensitive mechanical sensing unit [46–48]. However, the measurement accuracy of light intensity-modulated accelerometers is directly dependent on the stability of light intensity and has high requirements for the light source and its driver. Therefore, the cost of highly sensitive optical intensity-modulated optical accelerometers is high. The parameters of the structures and the optical accelerometer based on optical intensity modulation (i.e., resonant frequency, working frequency band, and sensitivity) are provided in Table 2.

Table 2. Parameters of the accelerometer based on optical intensity modulation.

Reference	Principle	Structure	Resonant Frequency (Hz)	Frequency Response Range (Hz)	Sensitivity
Kalenik et al. [31]	OWG	Cantilevered fiber optics	125	–	6%/g
Barbosa et al. [32]	OWG	Cantilevered fiber optics	3.3 k	20–2000	3.3 mV/g
Lee et al. [33]	OWG	Symmetrical flexure hinge	5.5 k	<1000	2.46 mV/g
Llobera et al. [34,35]	OWG	Symmetrical flexure hinge	51	–	32.14 dB/g
Schröpfer et al. [36]	OWG	Symmetrical flexure hinge	–	–	1.8 V/g
Cadarso et al. [37]	OWG	Symmetrical flexure hinge	–	–	13.1 dB/g
Abbaspour et al. [38]	GS	Flexure hinge	–	–	0.04 V/g
Wu et al. [39]	GS	Flexure hinge	60	10–1.5 k	–
Krishnamoorthy et al. [40]	GS	Flexure hinge	36	–	590 V/g
Bochobza et al. [44,45]	OSS	Cantilevered flexure hinge	550	<400	0.6 V/g
Hammond et al. [46]	OSS	Inverse spring	2.3	<0.02	41 ng/Hz$^{1/2}$
Tang et al. [47]	OSS	Asymmetric spring	3	<0.1	8.1 ng/Hz$^{1/2}$
Duan et al. [48]	OSS	V-shape elastic beam	8.24	<1	3800 µm/g

5. Optical Phase Modulation

Optical phase-modulated accelerometers use the phase change of an optical wave in an optical fiber caused by external vibrations to detect vibrations. Optical accelerometers based on optical phase modulation generally consist of two parts: an optical fiber interferometer and a vibration-sensitive elastic mechanism. Fiber optic interferometers can be classified into Michelson interferometers (MSIs), Mach–Zehnder interferometers (MZIs), and Fabry–Perot interferometers (FPIs) in accordance with the interference principle.

An MSI is a dual-beam interferometer in which coherent light from a laser is incident on two single-mode fibers, one of which is the detection fiber while the other is the reference fiber, as shown in Figure 12. Pechstedt et al. proposed an optical accelerometer by winding optical fibers on the top and bottom of an elastic cylinder with a mass block in the middle [49]. This accelerometer achieves differential vibration measurements and improved sensitivity, as shown in Figure 13a. Chen et al. fixed the detection fiber of an MSI to the seismic mass of an optical accelerometer. The mass is fixed onto the base of the accelerometer by elastic beams, as shown in Figure 13b. The frequency response range of this accelerometer is 5–500 Hz, which is a wide spectral response range [50,51]. In addition to elastic cylinders and elastic beams, elastic diaphragms with low resonance frequencies are also used as vibration-sensitive structures for optical accelerometers. Chen et al. achieved vibration measurement by fixing the detection fiber of an MSI onto a different elastic structure and using the bending stress of the diaphragm vibration to load onto the detection fiber and change its phase [52–54].

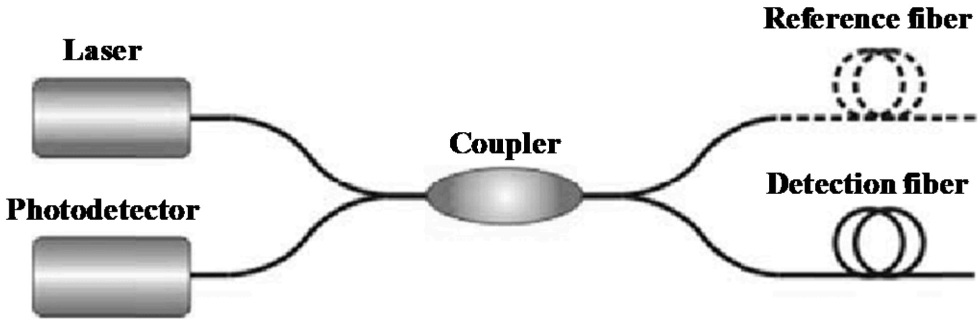

Figure 12. Schematic of the MSI.

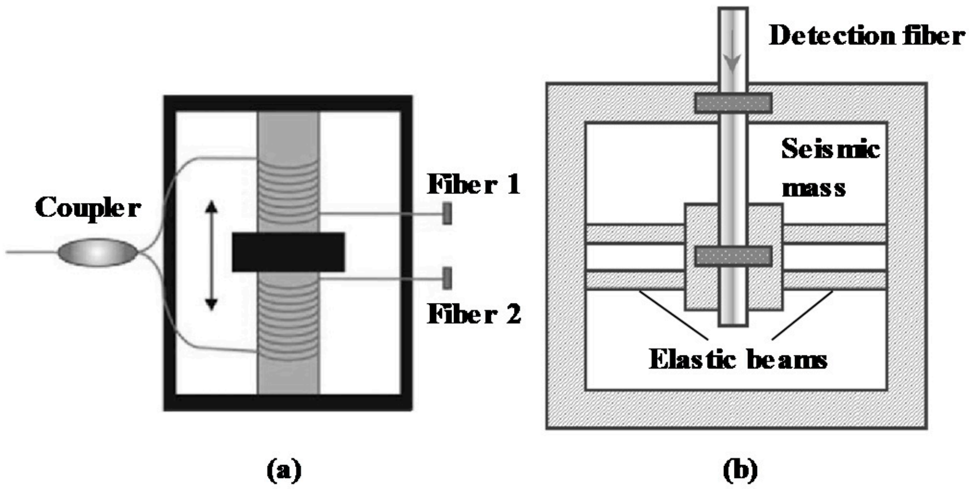

Figure 13. MSI-based accelerometer: (**a**) elastic cylinder and (**b**) elastic beam.

MZI is similar to MSI. Although both are two-beam interferometers, the difference is that MZI does not use end-face reflection, but instead, couples two beams to interfere for a transmission interferometer, as shown in Figure 14. The phase shift $\Delta\varphi$ from the strain caused by the acceleration a is

$$\varphi(a) = \frac{2\pi}{\lambda_0} n_f \Delta L(a), \tag{11}$$

where λ_0 is the wavelength of incident light, n_f is the effective refractive index of the optical fiber, and $\Delta L(a)$ is the amount of change in the detection fiber caused by the acceleration. The MZI optical accelerometer structure is also similar to that of MSI. Rivera et al. wrapped an optical fiber of MZI around the transformer core, and an acceleration value can be obtained by demodulating the change in the optical phase inside the fiber [55]. To improve the sensitivity of the MZI accelerometer, Rochus et al. fixed the detection fiber of the MZI interferometer in the form of a spiral on a diaphragm with a mass block to maximize the mechanical sensitivity of the MZI accelerometer, but the measurement range is small [56]. Zeng et al. proposed a 3D MZI optical accelerometer by mounting three-component optical accelerometers in orthogonal orientation [57]. Each single-component optical accelerometer is constructed by wrapping MZI detection fiber around an elastic cylinder, similar to the design of Pechstedt et al. [49]. The frequency response of this 3D optical accelerometer is within the range of 10–800 Hz. MZI and MSI exhibit similarities in measurement, sensor structure design, and signal demodulation. However, MSI exhibits two times the sensitivity of MZI when light wave makes one round trip in fiber with the same fiber length. In addition, MSI does not have a closed fiber loop and the fiber winding process is simpler. Therefore, MSI is more widely used than MZI.

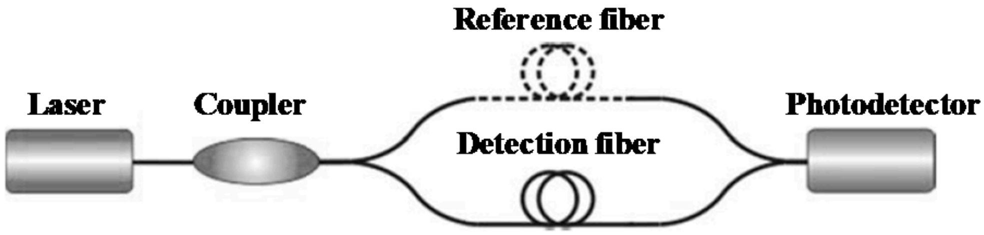

Figure 14. Schematic of the MZI.

In addition to MSI and MZI, which are two-optical interferometric sensing systems, the single-optical interferometric-based FPI is also widely used in optical accelerometers. The structure of FPI is shown in Figure 15. Its resonant cavity consists of two optical fiber end faces, wherein the incident light is reflected several times between the two end faces. The phase difference between two adjacent emitted lights is the same, and all reflected lights enter the detection system to produce multi-beam interference. The relationship between the end-face displacement ΔL and the phase shift $\Delta\varphi$ is

$$\Delta\varphi = \frac{4\pi n_f \Delta L}{\lambda_0}, \tag{12}$$

where λ_0 is the wavelength of the incident light, and n_f is the effective refractive index of the optical fiber.

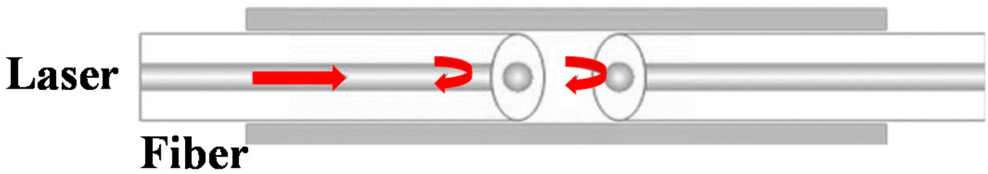

Figure 15. Schematic of the FPI.

Given that it is subject to acceleration, the inertial force of the seismic mass drives the end face of FPI, changing the reflection or transmission spectrum. The magnitude of input acceleration can be obtained by analyzing the spectrum. Gerges et al. proposed an optical accelerometer that consists of two identical hemispherical FPIs [58]. Two identical spherical metal mirrors are attached onto the central diaphragm (one on each side), forming the outer mirror of FPI, while the distal end of the fiber is used as the inner mirror. This optical accelerometer has a sensitivity of 2.2 × 10^{-7} g/$Hz^{1/2}$ and a resonant frequency of 450 Hz. Early FPI optical accelerometers exhibited high performance. In recent years, many researchers have started improving the mechanical design of optical accelerometers to increase their sensitivity. For example, Davies et al. introduced a V-beam displacement amplification structure into the accelerometer structure, as shown in Figure 16 [59]. The inertial displacement of the mass causes the V-shaped structure to compress in the x-direction and expand in the y-direction, modulating the Fabry–Perot cavity length and changing the wavelength of the output light. The bandwidth of this accelerometer is about 10 kHz, and the maximum mechanical amplification is 18.6.

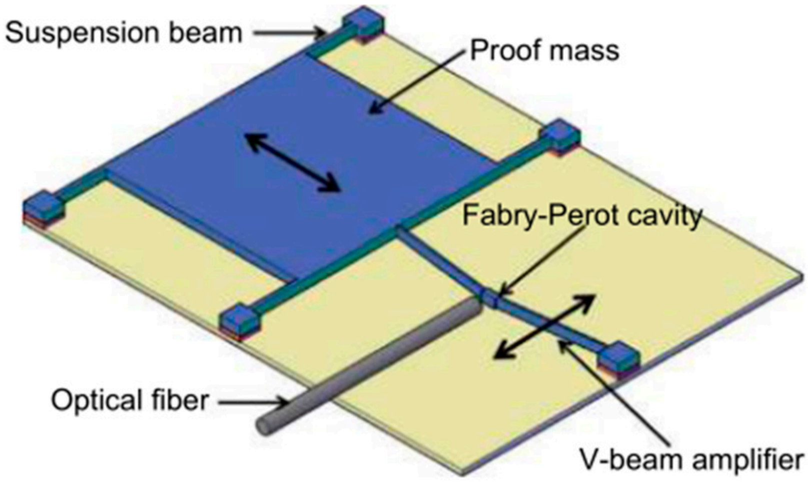

Figure 16. Schematic of a V-beam FPI-based accelerometer. Reprinted with permission from Ref. [59]. Copyright 2014 Elsevier.

Improving the resonant cavity of FPI is another strategy for increasing the sensitivity of an optical accelerometer in addition to improving its mechanical design. Cervantes et al. proposed an optical accelerometer based on an improved FPI that combines a parallelogram flexible oscillator and an optical fiber micro cavity [60]. This type of accelerometer can reach a sensitivity of 100 ng/Hz$^{1/2}$. Extending the length of the resonant cavity of FPI by a 45° reflector can also enhance the sensitivity of the accelerometer. This method allows the sensitivity of the accelerometer to be increased without affecting its resonant frequency [61,62]. Efforts must also be exerted to improve other properties of FPI optical accelerometers apart from their sensitivity. Multi-axis vibration detection is one research direction. Lin et al. designed a 3D optical accelerometer that was implemented by orthogonally mounting three 1D FPI optical accelerometers [63]. This accelerometer has a sensitivity of 48 ng/Hz$^{1/2}$ and a bandwidth of 160 Hz.

Micro-opto-electro-mechanical technology has developed rapidly in recent years, and phase-modulated accelerometers based on this technology have also gained the attention of researchers. In particular, grating interferometric accelerometers are developing rapidly. The core sensing unit of the grating interferometer (GI)-based accelerometer is the cavity of the grating interferometer. It is a micro-cavity composed of a movable diffraction grating. The cavity length is varied by modulating the optical range difference to change the intensity of the emitted light. However, the intensity modulation is susceptible to interference from low-frequency fluctuations in light intensity and changes in environmental conditions. To improve the signal quality, Zhao et al. proposed a grating interferometric accelerometer based on the demodulation method of phase and intensity dual modulation [64,65]. The optical accelerometer uses a micromechanical silicon structure based on a double-mask process as the elastic component and a photodetector with a sensitivity of 0.45 A/W for sensing. The sensitivity of the accelerometer has reached 619 V/g. A similar study was done by Lu et al. with good results [66–70], and the specific parameters are shown in Table 3.

In summary, optical accelerometers based on optical phase modulation exhibit the advantages of high sensitivity, compact structure, and simple optical path. The theoretical performance of optical accelerometers with optical phase modulation can be extremely high, and the corresponding acceleration measurement sensitivity can reach the sub-μg level. However, the performance of this type of optical accelerometer is directly related to the machining and assembly accuracy of its structure, and thus, such accelerometers require high micromachining accuracy and high cost but exhibit poor repeatability. They are suitable for high-precision military navigation or precision vibration isolation systems for precision instruments that are not cost-sensitive. The parameters of the structures and the optical accelerometer based on optical phase modulation (i.e., resonant frequency, working frequency band, and sensitivity) are provided in Table 3.

Table 3. Parameters of the accelerometer based on optical phase modulation.

Reference	Principle	Structure	Resonant Frequency (Hz)	Frequency Response Range (Hz)	Sensitivity
Pechstedt et al. [49]	MSI	Elastic cylinder	300	<100	–
Chen et al. [50,51]	MSI	Elastic beams	400	10–150	0.66 V/g
Chen et al. [52]	MSI	Elastic diaphragm	1.6 k	100–800	2.2 rad/g
Cranch et al. [59]	MSI	Elastic diaphragm	3.8 k	<1 k	35.9 dB re rad/g
Wu et al. [54]	MSI	Cantilever beam	490	10–300	1.13 V/g
Rochus et al. [56]	MZI	Elastic diaphragm	–	<25 k	–
Zeng et al. [57]	MZI	Elastic cylinder	1 k	10–800	38 dB re rad/g
Gerges et al. [58]	FPI	Elastic beams	450	<47.7	220 ng/Hz$^{1/2}$
Davies et al. [59]	FPI	Combined elastic beams	11.75 k	<5 k	0.3 mV/g
Cervantes et al. [60]	FPI	Parallelogram flexible oscillator	11 k	1.5–12 k	100 ng/Hz$^{1/2}$
Liu et al. [61,62]	FPI	Cantilever beam	520	20–160	20 V/g
Lin et al. [63]	FPI	Symmetrical leaf spring	144	20–120	36 dB re rad/g
Zhao et al. [64,65]	GI	Four cantilever beams	1 k	<200	619 V/g
Lu et al. [66]	GI	Four serpentine-shaped flexure beams	34.5	<5	2485 V/g
Zhang et al. [69]	GI	Eight cantilever beams	7553	100–2000	–
Yao et al. [70]	GI	Six serpentine-shaped flexure beams	24.8	<3	60 V/g

6. Optical Wavelength Modulation

Accelerometers based on optical wavelength modulation detect acceleration by measuring the wavelength drift of the output light under the effect of acceleration. The two main types of optical wavelength modulated accelerometers include fiber optic Bragg grating (FBG) accelerometers and photonic crystal (PHC) accelerometers.

Research on FBG started as early as 1978 [71,72]. FBG is a periodic modulation of the refractive index in the fiber core. When a broadband light is transmitted along with the fiber core, the FBG reflects the narrowband part of a specific wavelength while the rest of the broadband light passes through. The central wavelength of the reflected spectrum is defined as λ_b and can be expressed in terms of two parameters [73,74]:

$$\lambda_b = 2 * n_f * \Lambda, \tag{13}$$

where n_f is the effective refractive index of the optical fiber, and Λ is the periodicity of the grating. The wavelength shift of λ_b is decided by the changes of n_f and Λ, which are mainly influenced by the axial strain $\Delta\varepsilon$ and environment temperature ΔT. In this case, the Bragg wavelength dependency on the strain and temperature could be described by [75]

$$\frac{\Delta\lambda_b}{\lambda_b} = (1 - P_e) * \Delta\varepsilon + (\alpha_f + \xi) * \Delta T, \tag{14}$$

where α_f is the thermal expansion coefficient, ξ is the thermal optic coefficient, and P_e is the elastic optical coefficient.

Berkoff et al. designed an original FBG-based optical accelerometer, shown in Figure 17a, wherein the FBG is arranged in an elastic material [76]. The measurement of vibration is achieved by measuring the central wavelength drift of the FBG. This accelerometer has a sensitivity of 1 ng/Hz$^{1/2}$ and a bandwidth of 2 kHz. In addition to placing FBG inside an elastic material, fixing FBG onto an elastic beam has also been used in the design of optical accelerometers. The optical accelerometer designed by Todd et al. placed a seismic mass in the middle of two simply supported beams and fixed the FBG onto the lower surface of the lower simply supported beam, as shown in Figure 17b [77]. When external vibration is loaded onto the sensor, the deformation of the beam causes the center wavelength of the FBG to drift, and the amplitude and frequency information of the external vibration can be obtained on the basis of drift value. Mita et al. proposed an accelerometer with a cantilever FBG [78]. This accelerometer consists of an L-shaped rigid cantilever beam, a seismic mass, a spring, and FBG. In the design of Mita et al., FBG is not directly fixed onto the L-shaped cantilever beam, but instead, a point contact is used with the cantilever beam to ensure the consistency of the strain applied to the entire FBG. A similar design was made by Weng et al. [79,80].

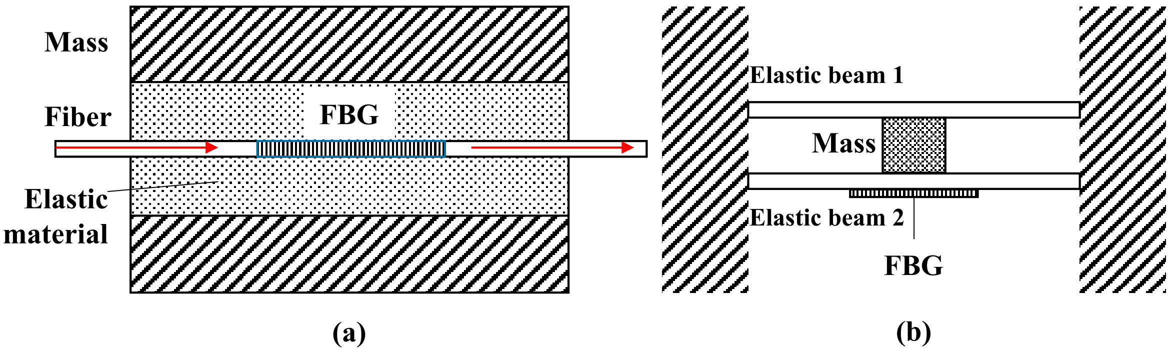

Figure 17. FBG-based accelerometer: (**a**) elastic material and (**b**) two simply supported beams.

FBG has good multipoint measurement capability. Linze et al. designed a distributed optical accelerometer based on FBG [81,82]. This distributed optical accelerometer is realized by using pairs of vibration-sensitive mechanical structures and paired FBGs with different Bragg wavelengths. In the design of Linze et al., up to six optical accelerometers can be combined for measurement.

In recent years, many researchers have started to focus on improving the performance of FBG optical accelerometers. In their research, they have exerted effort on two perspectives: the design of FBG and the design of a vibration-sensitive mechanical structure. Guo et al. used a tilted FBG (TFBG), as shown in Figure 18, to produce a biconical accelerometer, avoiding the difficulty of demodulation of the output optical wavelength signal when the traditional FBG accelerometer is used, and its reflected optical power is proportional to the acceleration [11]. A similar design was developed by Huang et al. [83]. The advantage of TFBG over FBG is that the optical fiber does not require stretching and can be embedded directly into the solid base, improving the reliability of the optical accelerometer and reducing its size.

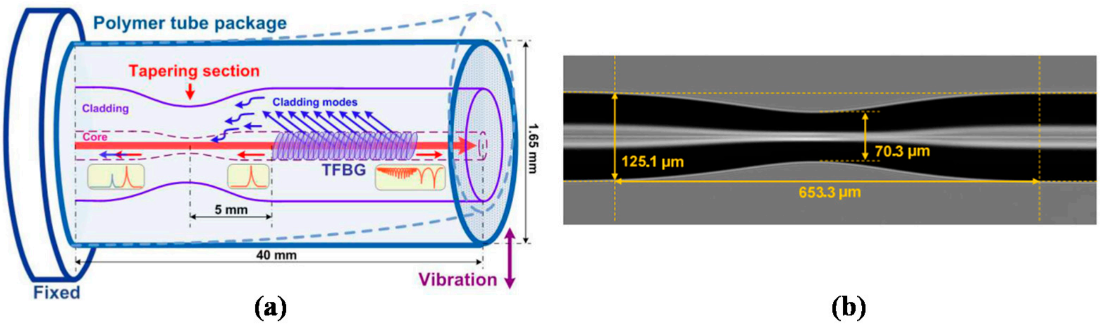

Figure 18. TFBG-based accelerometer [11]: (**a**) schematic and (**b**) photograph.

Other researchers have increased the sensitivity of FBG accelerometers by improving their mechanical design. As shown in Figure 19a, Basumallick et al. increased the sensitivity of a cantilever FBG accelerometer by using a simple method, i.e., adding a polyimide patch to the cantilever beam that does not affect its resonant frequency [84,85]. This polyimide patch increased the distance between the central axis of the cantilever beam and FBG, improving the sensitivity of the accelerometer. The design is simple in structure, but it improves sensitivity without affecting bandwidth and other characteristics. Shi et al.

and Yu et al. designed an FBG accelerometer based on an isosceles triangular cantilever beam [86,87]. Zhang et al. designed a compact accelerometer based on an organic double semicircular cantilever beam and double FBGs [88], as illustrated in Figure 19b. These studies were conducted to suppress the FBG chirp effect and improve the sensitivity of FBG optical accelerometers. Elastic diaphragms with high mechanical sensitivity have also been applied to FBG accelerometers. Liu et al. designed a double diaphragm-based FBG accelerometer with FBGs mounted on the upper surface of the diaphragm along the circumferential direction; this design can effectively prevent the FBG chirp effect [89]. When acceleration acts on the sensor, a uniform strain is generated, leading to an FBG wavelength shift.

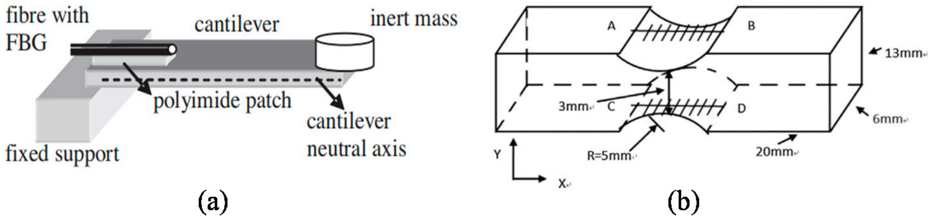

Figure 19. Improved cantilever FBG accelerometer: (**a**) polyimide patch and (**b**) double semicircular flexible hinge. Figures are reprinted with permission from: (**a**) Ref. [84]. Copyright 2012 Elsevier; (**b**) Ref. [88]. Copyright 2014 Elsevier.

The photonic crystal (PHC) accelerometer is also an optical wavelength modulated accelerometer. The displacement sensing unit of a PHC accelerometer is usually a one- or two-dimensional PHC waveguide. PHC waveguides have a photonic bandgap that is selective for the wavelength of the passing light [90]. Acceleration deforms the periodic photonic structure, thereby destroying and altering the selectivity. Thus, PHC accelerometers obtain acceleration values by detecting changes in wavelength.

PHCs can be classified into one-dimensional and two-dimensional forms depending on the form of lattice composition. One-dimensional PHCs are periodic stacks of materials with different refractive indices. When the periodicity or material properties of the bandgap material will be changed, the central wavelength of its output light will be changed. Sheikhaleh et al. used alternating silicon and air to form a bandgap PHC accelerometer with a mass connected to a silicon finger in the middle. When acceleration is applied to the accelerometer, the silicon finger in the middle moves in the sensing direction, thus changing the periodic condition of the bandgap, and the acceleration value can be obtained from the amount of change in the central wavelength of the output light [91]. A similar study was conducted by Huang et al. [92].

Mojtaba et al. proposed a two-dimensional PHC-based accelerometer consisting of two waveguides and a ring resonator with a two-dimensional rod-like PHC microstructure, and a holder connecting the central rod and mass of the nanocavity. When there is an acceleration acting on this accelerometer, the displacement of the mass causes the radius of the ring resonator to become larger, which results in a wavelength red-shift of the output resonant mode. By detecting the wavelength shift in the readout system, the magnitude and direction of the acceleration can be interpreted [93]. A similar study was conducted by Sheikhaleh et al. [94].

FBG accelerometers exhibit the advantages of anti-electromagnetic interference, low loss, good scalability, small size, and light weight. They can be applied in complex environments. In addition, FBG-based optical accelerometers provide an effective solution for realizing the multipoint monitoring of the health of the large infrastructure. However, as can be seen from Equation (14), the output signal of the FBG can be modulated by temperature compared to other types of optical modulation methods. Therefore, compared to other types of optically modulated accelerometers, FBG accelerometers have the highest sensitivity to ambient temperature and require temperature compensation when used. PHC accelerometers have the advantage of large bandwidth and compact size. However, their application and development are limited by manufacturing technology, and high-quality processing and material technology are prerequisites for achieving high sensitivity and high resolution in PHC [95]. In addition, the low-frequency response characteristics of PHC accelerometers have not been reported despite their large bandwidth.

Moreover, the detection of optical wavelengths relies on specialized high-precision instruments, and the readout output signal is complex and difficult to integrate and process. The parameters of the structures and the optical accelerometer based on optical wavelength modulation (i.e., resonant frequency, working frequency band, and sensitivity) are provided in Table 4.

Table 4. Parameters of the accelerometer based on optical wavelength modulation.

Reference	Principle	Structure	Resonant Frequency (Hz)	Frequency Response Range (Hz)	Sensitivity
Berkoff et al. [76]	FBG	Elastic material	2 k	<1 k	85 mrad/g
Todd et al. [77]	FBG	Two simply supported beams	1 k	10–100	212:5 $\mu\epsilon$/g
Mita et al. [78]	FBG	L-shaped rigid cantilever beam	49.2	<20	–
Linze et al. [81,82]	FBG	Simply supported beam	1.2 k	<1 k	0.10 V/g
Guo et al. [11]	TFBG	Cantilever beam	51	<30	8.3 nW/g
Huang et al. [83]	TFBG	Cantilever beam	–	<200	–
Basumallick et al. [84,85]	FBG	Cantilever beam	18.75	<10	1062 pm/g
Shi et al. [86]	FBG	Triangular cantilever beam	200	280–420	0.21 V/g
Zhang et al. [88]	FBG	Double semicircular flexible hinge	60	<25	1296.47 pm/g
Liu et al. [89]	FBG	Double-diaphragm	1240	50–800	45.9 pm/g
Sheikhaleh et al. [91]	PHC	Four serpentine-shaped flexure beams	8908	<2 k	1.17 nm/g
Huang et al. [92]	PHC	Four serpentine-shaped flexure beams	1037	0–900	1.07 μm/g
Sheikhaleh et al. [94]	PHC	Four serpentine-shaped flexure beams	12935	–	75 pm/g

7. Conclusions and Prospect

The accurate detection of low frequency (frequency below 10 Hz or even below 1 Hz) micro-vibration is of great significance for the development of high precision inertial navigation, structural health monitoring of large buildings, precision measurement/processing, wind turbine fault detection, earthquake detection, and other fields. The low-frequency micro-vibrations produce small acceleration amplitudes down to milligram or even microgram magnitude, requiring accelerometers with excellent low-frequency response characteristics. Accelerometers have made significant advances in recent decades. By taking advantage of optical modulation technology, accelerometers are currently capable of achieving impressive levels of performance.

This study analyzed the practical application requirements of optical accelerometers and then classified accelerometers into four categories: optical path, optical intensity, optical phase, and optical wavelength modulations. With the improvement in light source technology, photodetectors, optical signal modulation, and demodulation in recent years, the performance of accelerometers has been significantly improved, as evident in Tables 1–4. Each class of accelerometers exhibits advantages and disadvantages and are suitable for different requirements. For example, accelerometers based on optical path modulation and light intensity modulation typically have relatively simple optical path structures and signal processing circuits, as well as their mechanical structures being easy to design and machine, which easily improves their low-frequency response characteristics. However, their measurement accuracy depends on the performance of the light source and detector. In addition, the light source and detector are arranged internally in both types of optical accelerometers, making them complex, large, and heavy. The use of both types of optical accelerometers is suitable for applications wherein the size and mass requirements of the accelerometer are insensitive, such as precision active vibration isolation systems, structural health monitoring, and earthquake monitoring. Accelerometers based on optical phase and wavelength modulations have also been extensively investigated in recent years. The optical paths of these types of optical accelerometers are mostly arranged in optical fibers, while the light source and detector are placed outside. In addition, the mechanical structures of these two types of accelerometers are also mostly designed and processed using microelectromechanical techniques, with an overall compact structure and small size. However, these two types of accelerometers also have the problems of high cost and complicated output signal modulation and demodulation technology, and the convenience of using them is different from the first two types. Therefore, these types of accelerometers can measure micron-level acceleration with high accuracy in mass- and size-sensitive application scenarios, such as inertial navigation and wind turbine fault monitoring. A summary of the performance of the four types of optical accelerometers is provided in Table 5.

Table 5. Parameters of the four types of optical accelerometers.

Parameter	Optical Path Modulation	Optical Intensity Modulation	Optical Phase Modulation	Optical Wavelength Modulation
Optical displacement resolution	μm–nm scale	μm–nm scale	nm scale	nm scale
Characteristics	Simple optical path structure, signal processing circuits, and good low-frequency response		Compact structure, small size, and wide frequency response range	
Applications	Active vibration isolation systems, structural health monitoring, and earthquake monitoring		Inertial navigation and wind turbine fault monitoring	

Research on high-precision optical accelerometers will continue to flourish in the coming decades, focusing on the collaborative design of optical and mechanical components, the application of precision micromachining techniques, and the study of new optical measurement technologies. The development of high-precision optical accelerometers should be promoted toward high sensitivity, stability, integration, and anti-interference capability. Moreover, the application range of optical accelerometers should be broadened to make them convenient and easy-to-use precision instruments instead of being limited to laboratory application scenarios.

Author Contributions: Conceptualization, Y.-J.L. and R.-J.L.; methodology, L.-S.Z.; writing—original draft preparation, Y.-J.L.; writing—review and editing, R.-J.L., L.-S.Z. and P.-H.H.; funding acquisition, R.-J.L. and Q.-X.H. All authors have read and agreed to the published version of the manuscript.

Funding: This research was funded by the National Key R&D Program of China (2019YFB2004900) and the National Natural Science Foundation of China (52175506).

Institutional Review Board Statement: Not applicable.

Informed Consent Statement: Not applicable.

Data Availability Statement: Not applicable.

Conflicts of Interest: The authors declare no conflict of interest.

References

1. Shivashankar, P.; Gopalakrishnan, S. Review on the use of piezoelectric materials for active vibration, noise, and flow control. *Smart Mater. Struct.* **2020**, *29*, 053001. [CrossRef]
2. Pramanik, R.; Arockiarajan, A. Effective properties and nonlinearities in 1-3 piezocomposites: A comprehensive review. *Smart Mater. Struct.* **2019**, *28*, 103001. [CrossRef]
3. D'Alessandro, A.; Scudero, S.; Vitale, G. A review of the capacitive MEMS for seismology. *Sensors* **2019**, *19*, 3093. [CrossRef] [PubMed]

4. Giacci, F.; Dellea, S.; Langfelder, G. Signal integrity in capacitive and piezoresistive single-and multi-axis MEMS gyroscopes under vibrations. *Microelectron. Reliab.* **2017**, *75*, 59–68. [CrossRef]
5. Kordas, K.; Pitkänen, O. Piezoresistive carbon foams in sensing applications. *Front. Mater.* **2019**, *6*, 93. [CrossRef]
6. Liu, F.; Gao, S.; Niu, S.; Zhang, Y.; Guan, Y.; Gao, C.; Li, P. Optimal design of high-g MEMS piezoresistive accelerometer based on Timoshenko beam theory. *Microsyst. Technol.* **2018**, *24*, 855–867. [CrossRef]
7. Li, R.; Lei, Y.; Chang, Z.; Zhang, L.; Fan, K. Development of a high-sensitivity optical accelerometer for low-frequency vibration measurement. *Sensors* **2018**, *18*, 2910. [CrossRef]
8. Venkateshan, S.P. *Mechanical Measurements*; Springer: New York, NY, USA, 2015. [CrossRef]
9. Noureldin, A.; Karamat, T.; Georgy, J. *Fundamentals of Inertial Navigation, Satellite-Based Positioning and Their Integration*, 1st ed.; Springer: Berlin/Heidelberg, Germany, 2013. [CrossRef]
10. Antunes, P.; Lima, H.; Alberto, N.; Rodrigues, H.; Pinto, P.; Pinto, J.; Nogueira, R.; Varum, H.; Costa, A.; Andre, P. Optical fiber accelerometer system for structural dynamic monitoring. *IEEE Sens. J.* **2009**, *9*, 1347–1354. [CrossRef]
11. Guo, T.; Shao, L.; Tam, H.; Krug, P.; Albert, J. Tilted fiber grating accelerometer incorporating an abrupt biconical taper for cladding to core recoupling. *Opt. Express* **2009**, *17*, 20651–20660. [CrossRef]
12. Rivin, E. Vibration isolation of precision equipment. *Precis. Eng.* **1995**, *17*, 41–56. [CrossRef]
13. DeBra, D. Vibration isolation of precision machine tools and instruments. *CIRP Ann.* **1992**, *41*, 711–718. [CrossRef]
14. Liu, J.; He, J. Research on measurement of low-frequency and micro-amplitude of vibration in active damping of platform. *J. Univ. Shanghai Sci. Technol.* **2005**, *27*, 185–188. (In Chinese) [CrossRef]
15. Salameh, J.; Cauet, S.; Etien, E.; Sakout, A.; Rambault, L. Gearbox condition monitoring in wind turbines: A review. *Mech. Syst. Signal Processing* **2018**, *111*, 251–264. [CrossRef]
16. Amirat, Y.; Benbouzid, M.; Al-Ahmar, E.; Bensaker, B.; Turri, S. A brief status on condition monitoring and fault diagnosis in wind energy conversion systems. *Renew. Sustain. Energy Rev.* **2009**, *13*, 2629–2636. [CrossRef]
17. Igba, J.; Alemzadeh, K.; Durugbo, C.; Henningsen, K. Performance assessment of wind turbine gearboxes using in-service data: Current approaches and future trends. *Renew. Sustain. Energy Rev.* **2015**, *50*, 144–159. [CrossRef]
18. Teng, W.; Ding, X.; Tang, S.; Xu, J.; Shi, B.; Liu, Y. Vibration analysis for fault detection of wind turbine drivetrains—A comprehensive investigation. *Sensors* **2021**, *21*, 1686. [CrossRef]
19. Clinton, J.; Heaton, T. Potential advantages of a strong-motion velocity meter over a strong-motion accelerometer. *Seismol. Res. Lett.* **2002**, *73*, 332–342. [CrossRef]
20. Chu, C.; Lin, C. Development of an optical accelerometer with a DVD pick-up head. *Meas. Sci. Technol.* **2005**, *16*, 2498. [CrossRef]
21. Liu, Y.; Fan, K.; Chu, C.; Werner, A.; Gerd, J. Development of an optical accelerometer for low-frequency vibration using the voice coil on a DVD pickup head. *Meas. Sci. Technol.* **2008**, *19*, 084012. [CrossRef]
22. Li, R.; Chang, Z.; Lei, Y.; Cheng, Z.; Liu, X.; Fan, K.; Lv, J. A low-frequency micro accelerometer based on three-lobed leaf spring and a focus probe. *IEEE Photonics J.* **2019**, *11*, 6800712. [CrossRef]
23. Cheng, Z.; Liu, L.; Lei, Y.; Li, H.; Zhang, L.; Li, R.; Huang, Q. Modeling and improvement of a low-frequency micro-accelerometer. *Rev. Sci. Instrum.* **2021**, *92*, 025002. [CrossRef] [PubMed]
24. Li, R.; Xiang, M.; He, Y.; Fan, K.; Cheng, Z.; Huang, Q.; Zhou, B. Development of a high-precision touch-trigger probe using a single sensor. *Appl. Sci.* **2016**, *6*, 86. [CrossRef]
25. Zhang, L.; Long, Q.; Liu, Y.; Zhang, J.; Feng, Z. Correlation-steered scanning for scanning probe microscopes to overcome thermal drift for ultra-long time scanning. *Ultramicroscopy* **2016**, *166*, 16–26. [CrossRef] [PubMed]
26. Fan, K.; Li, R.; Xu, P. Design and verification of micro/nano-probes for coordinate measuring machines. *Nanomanufacturing Metrol.* **2019**, *2*, 1–15. [CrossRef]
27. Chu, C.L.; Lin, C.H.; Fan, K.C. Two-dimensional optical accelerometer based on commercial DVD pick-up head. *Meas. Sci. Technol.* **2006**, *18*, 265–274. [CrossRef]
28. Cheng, Z.; Liu, L.; Xu, P.; Li, R.; Fan, K.; Li, H.; Wei, Y. Modeling and Optimal Design for a High Stability 2D Optoelectronic Angle Sensor. *Sensors* **2019**, *19*, 4409. [CrossRef]
29. Lei, Y.; Li, R.; Chen, R.; Zhang, L.; Hu, P.; Huang, Q.; Fan, K. A high-precision two-dimensional micro-accelerometer for low-frequency and micro-vibrations. *Precis. Eng.* **2021**, *67*, 419–427. [CrossRef]
30. Fang, X.; Cao, M. Theoretical analysis of 2D acceleration laser sensor and several design parameters. *Opt. Laser Technol.* **2003**, *35*, 345–348. [CrossRef]
31. Kalenik, J.; Pająk, R. A cantilever optical-fiber accelerometer. *Sens. Actuators A* **1998**, *68*, 350–355. [CrossRef]
32. Barbosa, F.; Borin, F.; Arakaki, A.; Aguiar, J.; Chaves, C. A novel optical accelerometer. SBMO/IEEE MTT-S. In Proceedings of the International Conference on Microwave and Optoelectronics, Brasilia, Brazil, 25 July 2005. [CrossRef]
33. Lee, S.; Cho, D. Development of a micro-opto-mechanical accelerometer based on intensity modulation. *Microsyst. Technol.* **2004**, *10*, 147–154. [CrossRef]
34. Llobera, A.; Seidemann, V.; Plaza, J.; Cadarso, V.; Buttgenbach, S. Integrated polymer optical accelerometer. *IEEE Photonics Technol. Lett.* **2005**, *17*, 1262–1264. [CrossRef]
35. Llobera, A.; Seidemann, V.; Plaza, J.; Cadarso, V.; Buttgenbach, S. SU-8 optical accelerometers. *J. Microelectromech. Syst.* **2007**, *16*, 111–121. [CrossRef]

36. Schröpfer, G.; Elflein, W.; de Labachelerie, M.; Porte, H.; Ballandras, S. Lateral optical accelerometer micromachined in (100) silicon with remote readout based on coherence modulation. *Sens. Actuators A* **1998**, *68*, 344–349. [CrossRef]
37. Cadarso, V.; Llobera, A.; Villanueva, G.; Seidemann, V.; Buttgenbach, S.; Plaza, J. Polymer microoptoelectromechanical systems: Accelerometers and variable optical attenuators. *Sens. Actuators A* **2008**, *145*, 147–153. [CrossRef]
38. Abbaspour-Sani, E.; Huang, R.; Kwok, C. A novel optical accelerometer. *IEEE Electron Device Lett.* **1995**, *16*, 166–168. [CrossRef]
39. Wu, Y.; Kao, Y.; Chao, P.; Wey, C.; Sauter, T.; Eka, F.; Pandey, R. Design and Implementation of OLED Driving and OPD Readout Circuitry for an Optical Vibration Sensor. *IEEE Sens.* **2018**, 1–4. [CrossRef]
40. Carr, D.; Sullivan, J.; Friedmann, T. Femtophotonics: Optical transducers utilizing novel subwavelength dual layer grating structure. In Proceedings of the Solid-State Sensors, Actuators, and Microsystems Workshop, Hilton Head Island, SC, USA, 6–10 June 2004. [CrossRef]
41. Carr, D.; Sullivan, J.; Friedmann, T. Laterally deformable nanomechanical zeroth-order gratings: Anomalous diffraction studied by rigorous coupled-wave analysis. *Opt. Lett.* **2003**, *28*, 1636–1638. [CrossRef]
42. Krishnamoorthy, U.; Olsson Iii, R.H.; Bogart, G.R.; Baker, M.; Carr, D.; Swiler, T.; Clews, P. In-plane MEMS-based nano-g accelerometer with sub-wavelength optical resonant sensor. *Sens. Actuators A* **2008**, *145*, 283–290. [CrossRef]
43. Bramsiepe, S.; Loomes, D.; Middlemiss, R.; Paul, D.; Hammond, G. A high stability optical shadow sensor with applications for precision accelerometers. *IEEE Sens. J.* **2018**, *18*, 4108–4116. [CrossRef]
44. Bochobza-Degani, O.; Seter, D.; Socher, E.; Nemirovsky, Y. Comparative study of novel micromachined accelerometers employing MIDOS. *Sens. Actuators A* **2000**, *80*, 91–99. [CrossRef]
45. Bochobza-Degani, O.; Seter, D.; Socher, E.; Nemirovsky, Y. Design and noise consideration of an accelerometer employing modulated integrative differential optical sensing. *Sens. Actuators A* **2000**, *84*, 53–64. [CrossRef]
46. Middlemiss, R.; Samarelli, A.; Paul, D.; Hough, J.; Rowan, S.; Hammond, G. Measurement of the Earth tides with a MEMS gravimeter. *Nature* **2016**, *531*, 614–617. [CrossRef] [PubMed]
47. Tang, S.; Liu, H.; Yan, S.; Xu, X.; Wu, W.; Fan, J.; Liu, J.; Hu, C.; Tu, L. A high-sensitivity MEMS gravimeter with a large dynamic range. *Microsyst. Nanoeng.* **2019**, *5*, 1–11. [CrossRef] [PubMed]
48. Duan, Y.; Wei, X.; Wang, H.; Zhao, M.; Ren, Z.; Zhao, H.; Ren, J. Design and numerical performance analysis of a microgravity accelerometer with quasi-zero stiffness. *Smart Mater. Struct.* **2020**, *29*, 075018. [CrossRef]
49. Pechstedt, R.; Jackson, D. Design of a compliant-cylinder-type fiber-optic accelerometer: Theory and experiment. *Appl. Opt.* **1995**, *34*, 3009–3017. [CrossRef]
50. Chen, C.; Ding, G.; Zhang, D.; Cui, Y.; Li, S. Michelson fiberoptic accelerometer. *Rev. Sci. Instrum.* **1998**, *69*, 3123–3126. [CrossRef]
51. Chen, C.; Zhang, D.; Ding, G.; Cui, Y. Broadband Michelson fiber-optic accelerometer. *Appl. Opt.* **1999**, *38*, 628–630. [CrossRef]
52. Chen, G.; Zhang, X.; Brambilla, G.; Newson, T. Theoretical and experimental demonstrations of a microfiber-based flexural disc accelerometer. *Opt. Lett.* **2011**, *36*, 3669–3671. [CrossRef]
53. Cranch, G.; Nash, P. High-responsivity fiber-optic flexural disk accelerometers. *J. Lightwave Technol.* **2000**, *18*, 1233. [CrossRef]
54. Wu, X.; Wang, X.; Li, S.; Huang, S.; Ge, Q.; Yu, B. Cantilever fiber-optic accelerometer based on modal interferometer. *IEEE Photonics Technol. Lett.* **2015**, *27*, 1632–1635. [CrossRef]
55. Rivera, H.; García-Souto, J.; Sanz, J. Measurements of mechanical vibrations at magnetic cores of power transformers with fiber-optic interferometric intrinsic sensor. *IEEE J. Sel. Top. Quantum Electron.* **2000**, *6*, 788–797. [CrossRef]
56. Rochus, V.; Westerveld, W.J.; Figeys, B.; Figeys, B.; Rottenberg, X.; Jansen, R. Simulation and Design of an Optical Accelerometer. In Proceedings of the 20th International Conference on Thermal, Mechanical and Multi-Physics Simulation and Experiments in Microelectronics and Microsystems (EuroSimE), Hannover, Germany, 24–27 March 2019. [CrossRef]
57. Zeng, N.; Shi, C.; Zhang, M.; Wang, L.; Liao, Y.; Lai, S. A 3-component fiber-optic accelerometer for well logging. *Opt. Commun.* **2004**, *234*, 153–162. [CrossRef]
58. Gerges, A.; Newson, T.; Jackson, D. Practical fiber-optic-based submicro-g accelerometer free from source and environmental perturbations. *Opt. Lett.* **1989**, *14*, 1155–1157. [CrossRef]
59. Davies, E.; George, D.; Gower, M.; Holmes, A. MEMS Fabry–Pérot optical accelerometer employing mechanical amplification via a V-beam structure. *Sens. Actuators A* **2014**, *215*, 22–29. [CrossRef]
60. Guzmán Cervantes, F.; Kumanchik, L.; Pratt, J.; Taylor, J. High sensitivity optomechanical reference accelerometer over 10 kHz. *Appl. Phys. Lett.* **2014**, *104*, 221111. [CrossRef]
61. Liu, B.; Zhong, Z.; Lin, J.; Wang, X.; Liu, L.; Shan, M.; Jin, P. Extrinsic Fabry–Pérot cantilever accelerometer based on micromachined 45° angled fiber. *J. Lightwave Technol.* **2018**, *36*, 2196–2203. [CrossRef]
62. Han, J.; Zhang, W.; Wang, Z.; Sun, B.; Xu, B.; Li, F. Fiber optical accelerometer based on 45 degrees Fabry-Perot cavity. *Adv. Sens. Syst. Appl.* **2014**, *9274*, 927418. [CrossRef]
63. Lin, Q.; Chen, L.; Li, S.; Wu, X. A high-resolution fiber optic accelerometer based on intracavity phase-generated carrier (PGC) modulation. *Meas. Sci. Technol.* **2010**, *22*, 015303. [CrossRef]
64. Zhao, S.; Zhang, J.; Hou, C.; Bai, J.; Yang, G. Optical accelerometer based on grating interferometer with phase modulation technique. *Appl. Opt.* **2012**, *51*, 7005–7010. [CrossRef]
65. Zhao, S.; Hou, C.; Bai, J.; Yang, G.; Tian, F. Nanometer-scale displacement sensor based on phase-sensitive diffraction grating. *Appl. Opt.* **2011**, *50*, 1413–1416. [CrossRef]

66. Lu, Q.; Bai, J.; Wang, K.; He, S. Design, optimization, and realization of a high-performance MOEMS accelerometer from a double-device-layer SOI wafer. *J. Microelectromech. Syst.* **2017**, *26*, 859–869. [CrossRef]
67. Lu, Q.; Wang, C.; Bai, J.; Wang, K.; Lian, W.; Lou, S.; Jiao, X.; Yang, G. Subnanometer resolution displacement sensor based on a grating interferometric cavity with intensity compensation and phase modulation. *Appl. Opt.* **2015**, *54*, 4188–4196. [CrossRef]
68. Lu, Q.; Bai, J.; Wang, K.; Chen, P.; Fang, W.; Wang, C. Single Chip-based nano-optomechanical accelerometer based on subwavelength grating pair and rotated serpentine springs. *Sensors* **2018**, *18*, 2036. [CrossRef] [PubMed]
69. Zhang, T.; Liu, H.; Feng, L.; Wang, X.; Zhang, Y. Noise suppression of a micro-grating accelerometer based on the dual modulation method. *Appl. Opt.* **2017**, *56*, 10003–10008. [CrossRef]
70. Yao, Y.; Pan, D.; Wang, J.; Dong, T.; Guo, J.; Wang, C.; Geng, A.; Fang, W.; Lu, Q. Design and Modification of a High-Resolution Optical Interferometer Accelerometer. *Sensors* **2021**, *21*, 2070. [CrossRef] [PubMed]
71. Hill, K.; Fujii, Y.; Johnson, D.; Kawasaki, B. Photosensitivity in optical fiber waveguides: Application to reflection filter fabrication. *Appl. Phys. Lett.* **1978**, *32*, 647–649. [CrossRef]
72. Kawasaki, B.; Hill, K.; Johnson, D.; Fujii, Y. Narrow-band Bragg reflectors in optical fibers. *Opt. Lett.* **1978**, *3*, 66–68. [CrossRef]
73. Wang, X.; Guo, Y.; Xiong, L. Hybrid fiber Bragg grating sensor for vibration and temperature monitoring of a train bearing. *Chin. Opt. Lett.* **2018**, *16*, 070604. [CrossRef]
74. Wang, X.; Guo, Y.; Xiong, L.; Wu, H. High-frequency optical fiber Bragg grating accelerometer. *IEEE Sens. J.* **2018**, *18*, 4954–4960. [CrossRef]
75. Guo, T.; Zhang, T.; Li, Y.; Qiao, X. Highly sensitive FBG seismometer with a 3D-printed hexagonal configuration. *J. Lightwave Technol.* **2020**, *38*, 4588–4595. [CrossRef]
76. Berkoff, T.; Kersey, A. Experimental demonstration of a fiber Bragg grating accelerometer. *IEEE Photonics Technol. Lett.* **1996**, *8*, 1677–1679. [CrossRef]
77. Todd, M.; Johnson, G.; Althouse, B.; Vohra, S. Flexural beam-based fiber Bragg grating accelerometers. *IEEE Photonics Technol. Lett.* **1998**, *10*, 1605–1607. [CrossRef]
78. Mita, A.; Yokoi, I. Fiber Bragg grating accelerometer for buildings and civil infrastructures. Smart Structures and Materials 2001: Smart Systems for Bridges, Structures, and Highways. *Int. Soc. Opt. Photonics* **2001**, *4330*, 479–486. [CrossRef]
79. Weng, Y.; Qiao, X.; Guo, T.; Hu, M.; Feng, Z.; Wang, R.; Zhang, J. A robust and compact fiber Bragg grating vibration sensor for seismic measurement. *IEEE Sens. J.* **2011**, *12*, 800–804. [CrossRef]
80. Zeng, Y.; Wang, J.; Yang, H.; Ma, L. Fiber Bragg grating accelerometer based on L-shaped rigid beam and elastic diaphragm for low-frequency vibration measurement. *Acta Opt. Sin.* **2015**, *35*, 1206005. [CrossRef]
81. Linze, N.; Tihon, P.; Verlinden, O.; Mégret, P.; Wuilpart, M. Development of a multi-point polarization-based vibration sensor. *Opt. Express* **2013**, *21*, 5606–5624. [CrossRef]
82. Linze, N.; Tihon, P.; Verlinden, O.; Mégret, P.; Wuilpart, M. Linearity considerations in polarization-based vibration sensors. *Appl. Opt.* **2012**, *51*, 6997–7004. [CrossRef]
83. Huang, Y.; Guo, T.; Lu, C.; Tam, H. VCSEL-based tilted fiber grating vibration sensing system. *IEEE Photonics Technol. Lett.* **2010**, *22*, 1235–1237. [CrossRef]
84. Basumallick, N.; Chatterjee, I.; Biswas, P.; Dasgupta, K.; Bandyopadhyay, S. Fiber Bragg grating accelerometer with enhanced sensitivity. *Sens. Actuators A* **2012**, *173*, 108–115. [CrossRef]
85. Basumallick, N.; Biswas, P.; Dasgupta, K.; Bandyopadhyay, S. Design optimization of fiber Bragg grating accelerometer for maximum sensitivity. *Sens. Actuators A* **2013**, *194*, 31–39. [CrossRef]
86. Shi, C.; Zeng, N.; Ho, H.; Chan, C.; Zhang, M.; Jin, W.; Liao, Y. Cantilever optical vibrometer using fiber Bragg grating. *Opt. Eng.* **2003**, *42*, 3179–3181. [CrossRef]
87. Yu, Y.; Tam, H.; Chung, W.; Demokan, M. Fiber Bragg grating sensor for simultaneous measurement of displacement and temperature. *Opt. Lett.* **2000**, *25*, 1141–1143. [CrossRef] [PubMed]
88. Zhang, X.; Rong, Q.; Sun, H.; Yang, S.; Yuan, L.; Hu, M. Low-frequency fiber Bragg grating accelerometer based on a double-semicircle cantilever. *Opt. Fiber Technol.* **2014**, *20*, 190–193. [CrossRef]
89. Liu, Q.; Qiao, X.; Fu, H.; Gao, H.; Yu, D. Large frequency range and high sensitivity fiber Bragg grating accelerometer based on double diaphragms. *IEEE Sens. J.* **2014**, *14*, 1499–1504. [CrossRef]
90. Joannopoulos, J.; Villeneuve, P.; Fan, S. Photonic crystals: Putting a new twist on light. *Nature* **1997**, *386*, 143–149. [CrossRef]
91. Sheikhaleh, A.; Abedi, K.; Jafari, K. A proposal for an optical MEMS accelerometer relied on wavelength modulation with one dimensional photonic crystal. *J. Lightwave Technol.* **2016**, *34*, 5244–5249. [CrossRef]
92. Huang, K.; Nie, Y.; Liu, Y.; Liu, P.; Cao, L.; Wang, Q.; Li, J. A proposal for a high-sensitivity optical MEMS accelerometer with a double-mode modulation system. *J. Lightwave Technol.* **2021**, *39*, 303–309. [CrossRef]
93. Hosseinzadeh Sani, M.; Saghaei, H.; Mehranpour, M.; Asgariyan Tabrizi, A. A novel all-optical sensor design based on a tunable resonant nanocavity in photonic crystal microstructure applicable in MEMS accelerometers. *Photonic Sens.* **2021**, *11*, 457–471. [CrossRef]
94. Sheikhaleh, A.; Abedi, K.; Jafari, K. An optical MEMS accelerometer based on a two-dimensional photonic crystal add-drop filter. *J. Lightwave Technol.* **2017**, *35*, 3029–3034. [CrossRef]
95. Malayappan, B.; Lakshmi, U.; Rao, B.; Ramaswamy, K.; Pattnaik, P. Sensing Techniques and Interrogation Methods in Optical MEMS Accelerometers: A Review. *IEEE Sens. J.* **2022**, *22*, 6232–6246. [CrossRef]